

The evolution of the Eastern Himalayan syntaxis revealed by India (Tethyan Himalaya Series) in central Myanmar

Lothar Ratschbacher¹, Myo Min², Leander Franz³, Bradley R. Hacker⁴, Eva Enkelmann⁵, Eko Yoan Toreno⁶, Raymond Jonckheere⁶, Birk Härtel⁶, Bernd Dieter Schurr⁷, Marion Tichomirowa⁶, and Jörg A. Pfänder⁶

¹Geologie, Technische Universität Bergakademie Freiberg, 09599 Freiberg, Germany

²University of Mandalay

³Universität Basel

⁴University of California, Santa Barbara

⁵University of Calgary

⁶TU Bergakademie Freiberg

⁷Deutsches GeoForschungsZentrum GFZ

November 26, 2022

Abstract

In the Katha Range of central Myanmar, lithologic tracers and pressure-temperature-deformation-time data identify Cambro-Ordovician, Indian-affinity Tethyan Himalaya Series (THS), located ~700 km from their easternmost outcrop in S-Tibet and ~450 km from Himalayan rocks in the Eastern Himalayan Syntaxis (EHS). Metamorphism began at ~65 Ma, peaked at ~45 Ma (~510°C, 0.93 GPa), and exhumation/cooling (~25°C/Myr) occurred until ~30 Ma in a subduction-early collision setting. When the Burma microplate—part of the intra-Tethyan Incertus-arc—accreted to SE-Asia, its eastern boundary, the southern continuation of the Indus-Yarlung suture (IYS), was reactivated as the Sagaing fault (SF), which propagated northward into Indian rocks. In the Katha rocks, this strike-slip stage is marked by ~4°C/Myr exhumation/cooling. Restoring the SF system defines a continental collision-oceanic subduction transition junction, where the IYS bifurcates into the SF at the eastern edge of the Burma microplate and the Jurassic ophiolite-Jadeite belt that includes the Incertus suture.

1 **The evolution of the Eastern Himalayan syntaxis revealed by**
2 **India (Tethyan Himalaya Series) in central Myanmar**

3

4 **Myo Min^{1,2}, Lothar Ratschbacher¹, Leander Franz³, Bradley R. Hacker⁴, Eva**
5 **Enkelmann⁵, Eko Yoan Toreno¹, Raymond Jonckheere¹, Birk Härtel¹, Bernd**
6 **Schurr⁶, Marion Tichomirowa¹, Jörg A. Pfänder**

7

8 ¹Geowissenschaften, TU Bergakademie Freiberg, Freiberg, Germany, ²Geology Department, University of
9 Mandalay, Mandalay, Myanmar, ³Mineralogisch-Petrologisches Institut, Universität Basel, Basel,
10 Switzerland, ⁴Geological Sciences, University of California, Santa Barbara, USA, ⁵Department of
11 Geosciences, University of Calgary, Alberta, Canada, ⁶German Research Center for Geoscience, Potsdam,
12 Germany

13

14 Corresponding author: Lothar Ratschbacher (lothar@geo.tu-freiberg.de)

15

16 **Key Points:**

- 17 • Indian-affinity Tethyan Himalaya Series occur in central Myanmar, ~450 km south
18 of the Himalayan rocks in the Eastern Himalayan Syntaxis
- 19 • A low temperature-high pressure subduction-early collision setting was active at
20 ~65 Ma, peaked at ~45 Ma, and ended at ~30 Ma
- 21 • The Sagaing transform fault reactivated the Indus-Yarlung suture, and imbricated
22 the Indian rocks and the Burma microplate from ~30 Ma on

23

24

25 **Abstract**

26 In the Katha Range of central Myanmar, lithologic tracers and pressure-temperature-
27 deformation-time data identify Cambro-Ordovician, Indian-affinity Tethyan Himalaya
28 Series (THS), located ~700 km from their easternmost outcrop in S-Tibet and ~450 km
29 from Himalayan rocks in the Eastern Himalayan Syntaxis (EHS). Metamorphism began at
30 ~65 Ma, peaked at ~45 Ma (~510°C, 0.93 GPa), and exhumation/cooling (~25°C/Myr)
31 occurred until ~30 Ma in a subduction-early collision setting. When the Burma
32 microplate—part of the intra-Tethyan Incertus-arc—accreted to SE-Asia, its eastern
33 boundary, the southern continuation of the Indus-Yarlung suture (IYS), was reactivated
34 as the Sagaing fault (SF), which propagated northward into Indian rocks. In the Katha
35 rocks, this strike-slip stage is marked by ~4°C/Myr exhumation/cooling. Restoring the SF
36 system defines a continental collision-oceanic subduction transition junction, where the
37 IYS bifurcates into the SF at the eastern edge of the Burma microplate and the Jurassic
38 ophiolite-Jadeite belt that includes the Incertus suture.

39

40 **Plain Language Summary**

41 Central Myanmar hosts rocks typical for the northernmost continental crust of the Indian
42 continent. These rocks are now located ~700 km from their easternmost outcrop in S-
43 Tibet and ~450 km from Himalayan rocks in the Eastern Himalayan Syntaxis—the
44 eastern edge of India. They record an oceanic subduction-early collision setting from ~65
45 to 30 Ma. Our findings aid to the restoration of the Sagaing transform-fault (SF) system
46 at the eastern edge of India. The SF system imbricated the Indian-affinity rocks, and the
47 Burma microplate—part of the intra-Tethyan Incertus-arc.

48

49

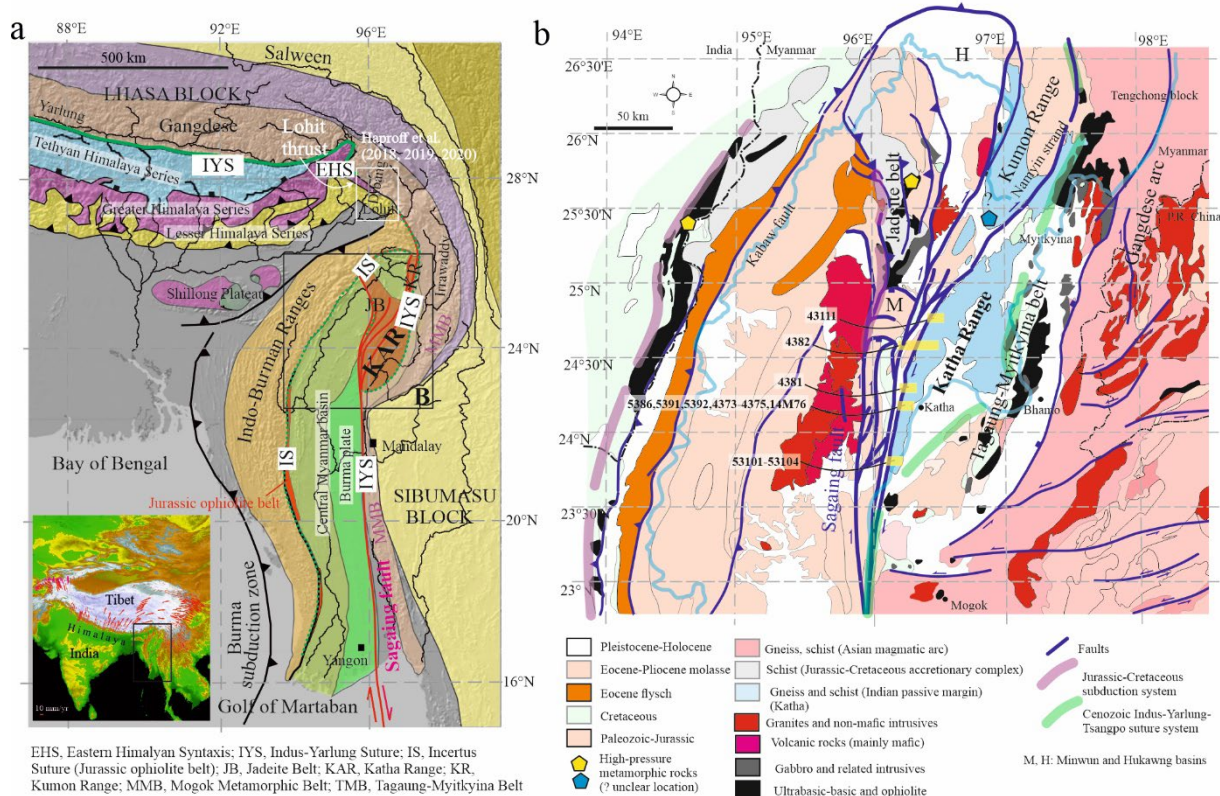
50 **1. Introduction**

51

52 Indenter corners in collisional orogens—syntaxes—feature 3-D deformation with crustal
53 thickening, lateral material flow, and transitions from continental to oceanic subduction.
54 In the Cenozoic India-Asia collision zone, the underthrusting Indian craton has induced
55 shortening in the Himalaya and Tibet, and lateral material flow out of the collision zone
56 (e.g., [Zhang et al., 2004](#); [Zubovich et al., 2010](#)). Pronounced lateral flow and clockwise
57 vertical-axis rotations occur at the Eastern Himalayan Syntaxis (EHS) where the
58 Himalayan continental subduction transitions into the highly-oblique Burma oceanic
59 subduction zone and the Sagaing transform-fault (SF) system ([Figure 1a](#)). Paleomagnetic
60 studies in the Burma microplate, and the Asian-affinity Tengchong (Lhasa) and Baoshan
61 (Qiangtang-Sibumasu) blocks indicate 40–90° clockwise, vertical-axis rotations in
62 Myanmar and Yunnan since the Paleocene, changing the original ~W-strike of these
63 blocks in Tibet to a ~N-strike south of the EHS (e.g., [Kornfeld et al., 2014](#); [Li et al., 2018](#),
64 [2020](#); [Westerweel et al., 2019](#)).

65

66 Northward-widening cratonic India extends northeastward into the EHS region, and is
67 rimmed in the east by the oceanic lithosphere of the Bay of Bengal. The current transition
68 from continental collision to oceanic subduction must occur in the Indo-Burman Ranges
69 (IBR), part of the Jurassic-Recent subduction-accretionary wedge that bounds the Indian
70 plate in the east, because the footwall of the northern IBR is made up of the Indian
71 continental crust of the Shillong Plateau ([Figure 1a](#)). The past position of this transition is
72 unclear due to the intervening Burma microplate and the northward-growing SF system,
73 disrupting the Burma microplate, the IBR wedge, and the southern prolongation of the
74 Indus-Yarlung suture (IYS) between India and Asia (e.g., [Baxter et al., 2011](#)).



75

76 **Figure 1. a)** Eastern Himalayan Syntaxis and eastern margin of the Indian plate (modified from [Robinson](#)
 77 [et al., 2014](#)). Insert locates a) and shows Eurasia-fixed GNSS-derived displacement field. b) Geological map
 78 centered on the Katha Range modified from [Geological Map of Myanmar \(2014\)](#) and [Wang & Burchfiel](#)
 79 [\(1997\)](#). Sagaing transform-fault system modified from [Morley & Arboit \(2019\)](#) and [Maurin et al. \(2010\)](#).
 80 Yellow bars: studied traverses and samples.

81

82 To account for the ≥ 50 Ma onset of the India-Asia collision (e.g., [Hu et al., 2016](#)), a northern
 83 extension of cratonic India has been proposed. This Greater India is envisioned as a
 84 < 2000 -km-wide northward-projecting entity, consisting of extended continental and
 85 oceanic Indian lithosphere (e.g., [van Hinsbergen et al., 2012](#)) that has along its northern
 86 rim the Tethyan Himalaya Series (THS), on which the ophiolites of the IYS were emplaced.

87

88 Given that India's northward motion has been accommodated by subduction/shortening
 89 of Greater Indian and cratonic Indian lithosphere, lateral material flow out of the collision

90 zone, and northward propagation of the Burma subduction zone and the SF system,
91 tracing the evolution of the continental collision-oceanic subduction transition,
92 describing the initiation and evolution of the SF system, and reconstructing the eastern
93 edge of Greater India are key aspects of understanding the India-Asia collision zone and
94 of indenter corners in general. Here, we trace the eastern edge of India—represented by
95 the THS—into central Myanmar. In the Katha Range, lithologic tracers and pressure-
96 temperature-deformation-time (P-T-d-t) data outline a piece of the basal Cambro-
97 Ordovician THS that experienced high-P–low T metamorphism, exhumed rapidly in a
98 subduction-early collisional setting, and was involved into the northward growth of the
99 SF system. The Katha rocks allow the timing of the activity in the subduction-early
100 collisional setting and of the onset of strike-slip faulting along the SF system, and aid in
101 the restoration of the eastern margin of India.

102

103 **2. The eastern Himalayan Syntaxis Region**

104

105 [Haproff et al. \(2018, 2019, 2020\)](#) and [Salvi et al. \(2019\)](#) mapped the lithologic units of
106 India and Asia at the EHS (Dibang and Lohit valleys; [Figure 1a](#)), encountering the
107 Gangdese arc (Asia), the IYS (Tidding-Mayoda mélangé), and the Lesser Himalaya Series
108 (LHS; India, Mayodia gneiss, Lalpani schist). The Greater Himalaya Series (GHS), THS, and
109 Xigaze forearc basin (Asia) are absent.

110

111 The NNE-trending Katha Range ([Figure 1b](#)) is bounded in the east by the 177–163 Ma (U-
112 Pb zircon) Tagaung-Myitkyina suprasubduction-zone (ultra-)mafic rocks ([Yang et al.,](#)
113 [2012; Liu et al., 2016](#)), which are intruded by Gangdese-arc granitoids ([Zhang et al., 2018](#)).

114 In the west, the Range is bounded by the Namyin strand of the SF system; rocks involved

115 in its western strands include the Jurassic (Qiu et al., 2009; Shi et al., 2008) Jadeite belt
116 (Figure 1b). Sericite-chlorite-biotite-garnet schist, locally with amphibole, talc, and
117 kyanite, quartzite, and marble have been reported from the Katha Range; their
118 stratigraphic age may cover the early Paleozoic to Triassic (e.g., Mitchell, 2018; Zhang et
119 al., 2018).

120

121 **3. Katha Range: Lithology, Pressure-temperature-deformation-time**

122 **Evolution**

123

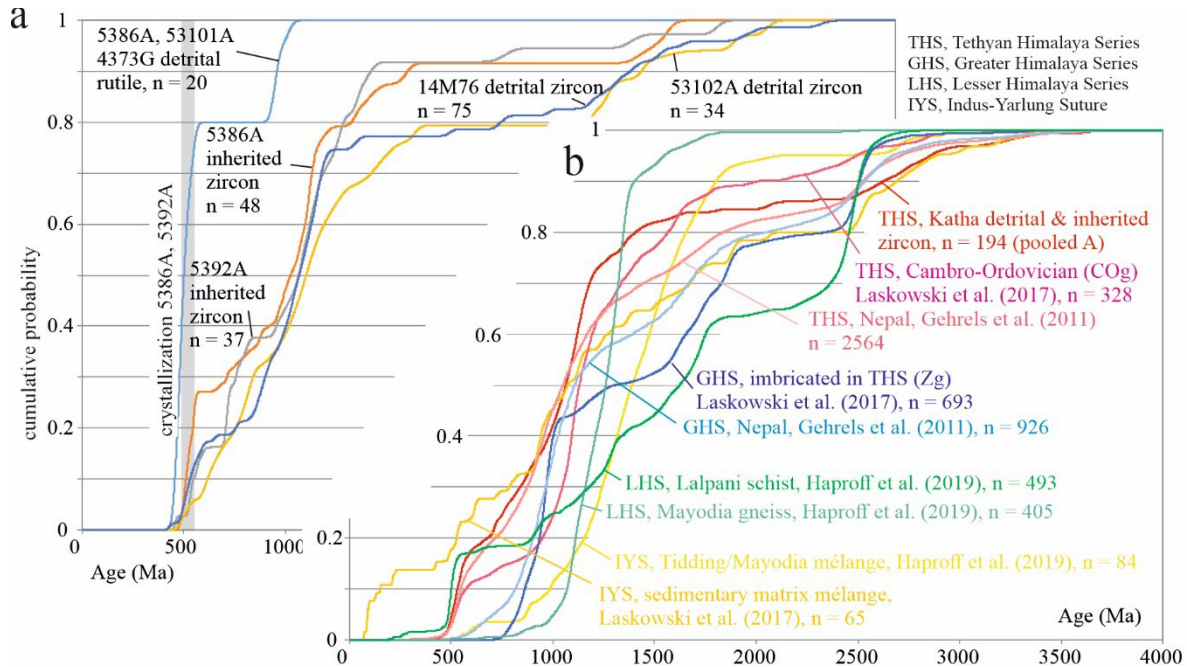
124 Lithologically, we encountered porphyroblastic chloritoid-garnet-graphite micaschist,
125 chlorite-chloritoid-bearing white-mica quartzite, and porphyroblastic staurolite-kyanite-
126 garnet quartz micaschist. Locally, the Katha schists and quartzites enclose m-thick meta-
127 acidite tectonites, dominated by phengite and porphyric quartz, interpreted as volcanic
128 layers or small hypabyssal intrusions. We used zircon and rutile U-Pb geochronology to
129 determine igneous emplacement ages, the maximum deposition age of the meta-
130 sedimentary rocks, and to establish correlations with rocks of the Himalaya and S-Tibet.
131 Supporting information Text S1 provides the sample petrography, Text S2 outlines the
132 geo-thermochronologic methods, and Tables S1 to S3 list their results and analytical data.

133

134 Two meta-acidites yielded U-Pb zircon crystallization ages of 501 ± 9 and 530 ± 5 Ma (2s;
135 Figure S1 in Supporting Information), both with major inheritance. Figure 2a compares
136 the inherited (meta-acidites) and detrital (meta-sedimentary rocks) U-Pb zircon and
137 rutile ages: the zircon age distributions of all samples are consimilar, with clusters at
138 ~ 500 and 1000 Ma; nearly all detrital rutile ages are at ~ 500 Ma. The youngest detrital
139 zircon and rutile grains are $482 +7/-19$ and $463 +8/-10$ Ma, respectively, calculated with

140 the “Youngest Zircon” routine and “3rd degree of youngest option” (Isoplot4.5; Ludwig,
 141 2008). These dates suggest a Cambro-Ordovician age for the studied Katha rocks.

142



143

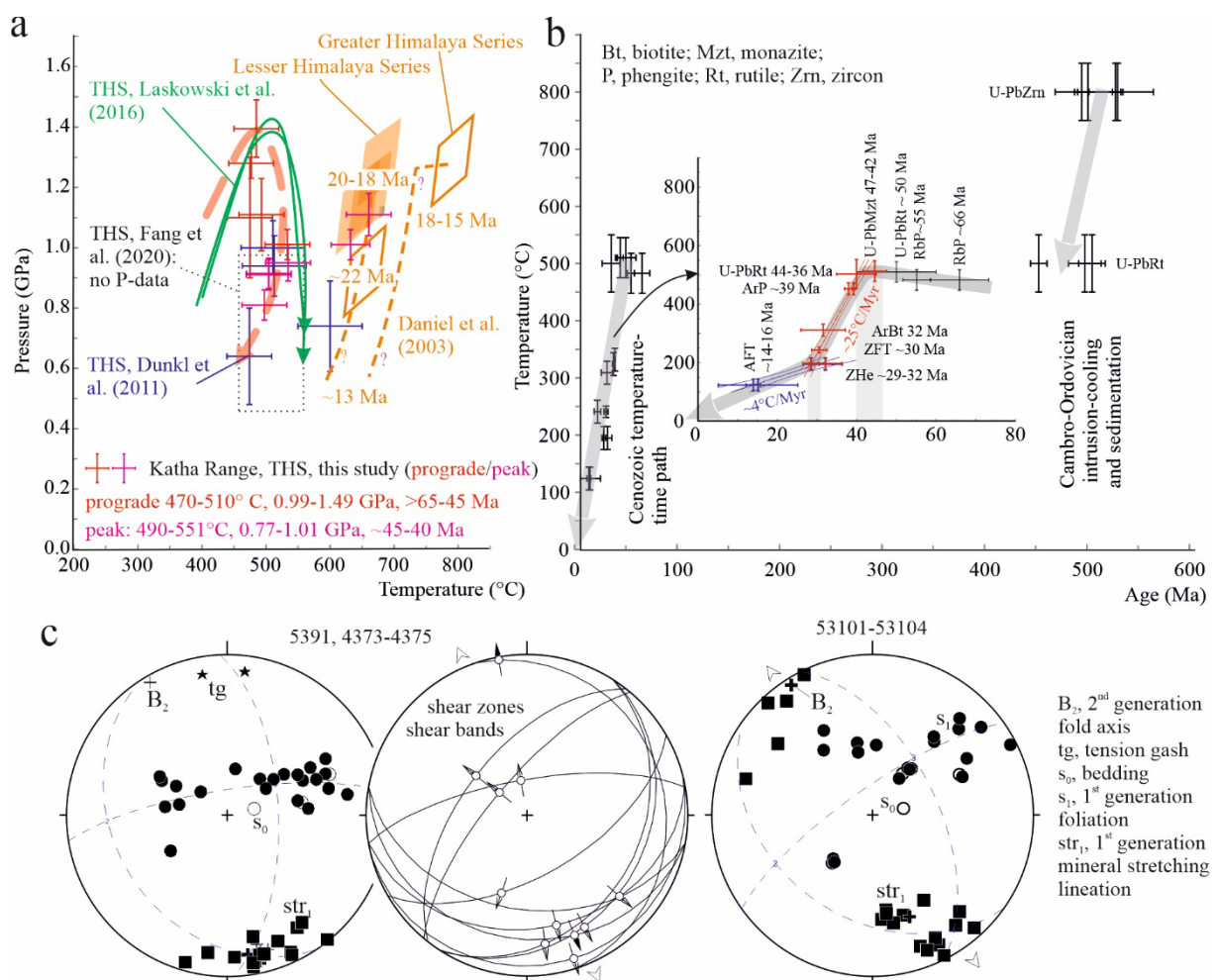
144 **Figure 2.** Cumulative probability plots of U-Pb zircon and rutile ages of a) samples from this study and
 145 sample 14M76 of Zhang et al. (2018), and b) their comparison with rocks from the central and eastern
 146 Himalaya. Ages used include 2s uncertainties and have 90–110% ²⁰⁶Pb/²³⁸U–²⁰⁷Pb/²⁰⁶Pb age concordance.

147

148 **Figure 3a** plots the Katha-rock P-T data together with THS data from central S-Tibet
 149 (Laskowski et al., 2016), eastern S-Tibet (Dunkl et al., 2011, Fang et al., 2020), and GHS
 150 and LHS data from Bhutan (Daniel et al., 2003). Table S4 of the Supporting Information
 151 summarizes our P-T results, and Text S1 details the petrology, derived from
 152 THERIAK/DOMINO equilibrium-assemblage calculations and conventional
 153 thermobarometry. Four meta-sedimentary rocks yielded prograde P-T data of 470–
 154 510°C, 1.0–1.5 GPa and peak data at 490–551°C, 0.8–1.0 GPa; one sample has higher
 155 temperatures (prograde ~535°C, 1.0 GPa, peak ~650°C, 1.0 GPa). Figure 3b plots the
 156 Katha-rock T-t history. The meta-acidite zircon ages, the youngest detrital zircon age
 157 groups, and the detrital rutile ages (all U-Pb) indicate a Cambro-Ordovician intrusion

158 (zircon) and cooling (rutile) event. U-Pb monazite and rutile, Rb-Sr phengite, $^{40}\text{Ar}/^{39}\text{Ar}$
 159 phengite and biotite, zircon (ZFT) and apatite fission track (AFT), and zircon (U-Th)/He
 160 (ZHe) dates outline the Cenozoic evolution. We calculated closure-temperatures, T_c , with
 161 CLOSURE (Brandon et al., 1998). For Ar/Ar phengite, we used a T_c of $\sim 450^\circ\text{C}$, accounting
 162 for slower diffusional loss at elevated pressures (e.g., Harrison et al., 2009; Warren et al.,
 163 2012). Changes in the actual T_c have little effect on the first-order T-t history.

164



165

166 **Figure 3.** Pressure-temperature-time-deformation (P-T-t-d) data. a) P-T of the Katha rocks and comparison
 167 with data from central and eastern S-Tibet and the eastern Himalaya. b) T-t paths, and c) structural data of
 168 the Katha rocks; see Figure 1b for traverses studied.

169

170 Given a $\sim 550^\circ\text{C}$ T_c for the Rb-Sr phengite system (e.g., [Blanckenburg et al., 1989](#))—higher
171 than the average peak-T ($\sim 510^\circ\text{C}$)—the two dates ≥ 55 Ma likely are formation ages
172 during prograde metamorphism ($\sim 483^\circ\text{C}$ average T). The same may apply for the U-Pb
173 rutile date (~ 50 Ma; T_c of $500\text{--}650^\circ\text{C}$; e.g., [Kooijman et al., 2010](#); [Ewing et al., 2015](#)) of
174 quartzite 53101A, whose $500\text{--}800^\circ\text{C}$ T-range from Zr-in-rutile isopleths ([Figure S1](#) of
175 Supporting Information) indicates incomplete reset of detrital rutile. The $500\text{--}550^\circ\text{C}$ Zr-
176 in-rutile-derived T-range of $44\text{--}36$ Ma rutiles indicates metamorphic growth in meta-
177 acidite 5386A, different from the higher-T of inherited grains ([Figure S1](#) of Supporting
178 Information). Peak-T is likely best dated by the $48\text{--}42$ Ma monazite inclusions ($\sim 10\ \mu\text{m}$)
179 in poikiloblastic kyanite of sample 4382. Taken together, the T-t path comprises prograde
180 metamorphism from ~ 65 Ma to peak P-T at ~ 45 Ma (~ 55 km burial, assuming a lithostatic
181 gradient of ~ 37 km/GPa), cooling at $\sim 25^\circ\text{C}/\text{Myr}$ to ~ 30 Ma, and cooling at $\sim 4^\circ\text{C}/\text{Myr}$
182 thereafter ([Figure 3b](#)).

183

184 [Figure 3c](#) compiles structural data of the Katha rocks along two traverses. Bedding (s_0)
185 and foliation (s_1) occupy a great-circle distribution, recording open to tight folds with
186 \sim NNW-trending axes (B_2), subparallel to mineral stretching lineation str_1 . S_1 and str_1 are
187 associated with folded shear zones/bands that indicate \sim NNW-SSE stretch with dominant
188 top-to-SSE shear, also indicated by σ -clasts and asymmetric foliation boudinage.
189 Overprinting a relict fabric, s_1 , str_1 , and the shear fabrics are outlined by the syn- to post-
190 peak P-T mineral assemblage; they likely record exhumation by crustal extension. The
191 folds record the regional \sim E-W shortening south of the EHS (e.g., [Wang & Burchfiel, 1997](#)).

192

193 **3. Discussion**

194

195 We focus on four salient questions: What Himalaya-Tibet series do the Katha rocks
196 represent? How and when were they exhumed? Which position did they occupy in the
197 evolution of the India-Asia collision system? When and how were they involved in the
198 oblique plate boundary south of the EHS?

199

200 Lithologically, the Katha rocks are part of the THS and most similar to the Cambro-
201 Ordovician gneiss-schist unit in central S-Tibet (Laskowski et al., 2017). Figure 2b
202 compares the inherited and detrital zircon ages of the Katha rocks with equivalents, i.e.,
203 the Cambro-Ordovician THS of central S-Tibet, the Nepal THS, the central Himalaya and
204 Nepal GHS, the LHS units at the EHS, the IYS in the central Himalaya and at the EHS
205 (Gehrels et al., 2011; Laskowski et al., 2016; Haproff et al., 2019); we chose these units
206 because of their proximity to the EHS, P-T-t-d history (central Himalaya), and large
207 database (Nepal). The Katha rocks compare best to the THS, and least to the IYS, LHS, and
208 GHS rocks.

209 Petrologically, the Katha-rock data (Figure 3a; red P-T path) are most similar to the
210 THS data of central S-Tibet (Figure 3a; green P-T paths; Laskowski et al., 2016); there,
211 metamorphism at ≥ 1.4 GPa, $\leq 600^\circ\text{C}$ peaked at ~ 40 Ma and the rocks cooled rapidly
212 through 39–34 Ma. The basal THS rocks of eastern S-Tibet experienced comparable-T but
213 lower-P ($\sim 600^\circ\text{C}$, 0.78 GPa; Dunkl et al., 2011; $510 \pm 50^\circ\text{C}$, Fang et al., 2020; Figure 3a)
214 and burial-early exhumation histories like those inferred for Katha (~ 49 –32 Ma; U-Pb
215 zircon, K(Ar)/Ar mica; e.g., Ratschbacher et al., 1994; Aikman et al., 2008, 2012; Dunkl et
216 al., 2011). Post-thrusting uppermost GHS granitoids in the same area have 48–36 Ma U-
217 Pb zircon ages; the associated schists show higher-T and lower-P (~ 630 –660 $^\circ\text{C}$, 0.7–0.8
218 GPa; Ding et al., 2016a, b) than the Katha rocks. Different from the latter, both the THS and
219 GHS rocks experienced Miocene rapid cooling (~ 18 –12 Ma; e.g., Aikman et al., 2008, 2012;

220 [Dunkl et al., 2011](#); [Ding et al., 2016a](#)). The IYS rocks of the southern EHS (Tidding-Mayodia
221 mélangé) record metamorphism and $\sim 30^{\circ}\text{C}/\text{Myr}$ cooling between 40–30 Ma and rapid
222 Miocene cooling ($\sim 11\text{--}6$ Ma; ZHe ages; [Haproff et al., 2020](#)), not documented in the Katha
223 rocks. The Katha P-T-t data contrast with GHS and LHS data in Bhutan ([Figure 3a](#); e.g.,
224 [Daniel et al., 2003](#)). Lithology and P-T-t evolution are compatible with the Katha rocks
225 being a piece of the basal—Cambro-Ordovician—THS, now located ~ 700 km of the THS
226 in eastern S-Tibet and ~ 450 km south of the Himalayan rocks in the Lohit valley at the
227 southern edge of the EHS.

228

229 Structural studies in eastern S-Tibet outlined top-to-S thrusts and S-facing folds,
230 overprinted by N-facing folds close to the Great Counter Thrust along the IYS (e.g.,
231 [Ratschbacher et al., 1994](#); [Dunkl et al., 2011](#)). Detachments—most with top-to-N
232 kinematics—separate the GHS and THS and occur within the basal THS (e.g., [Ding et al.,](#)
233 [2016a,b](#)). In the southern EHS, [Haproff et al. \(2018\)](#) mapped thrusts with a $\leq 90^{\circ}$ clockwise
234 change in displacement directions. The Katha rocks preserve—besides relict
235 deformation—fabrics akin to the normal-sense detachments in the THS. Assuming 60–
236 90° clockwise rotation due to the motion of the Himalayan (THS of Katha) and Asian
237 (Tengchong–Gangdese) rocks of central and eastern Myanmar and Yunnan around the
238 EHS, the top-to-SSE flow in the Katha THS rocks restores to top-to- \sim E flow, deflected $\sim 90^{\circ}$
239 from the typical top-to-N flow in S-Tibet. The younger, \sim NNW-trending folds parallel the
240 present-day structural grain and appear unrotated.

241

242 Whereas the exhumation history is comparable to other THS localities, two aspects of the
243 Katha rocks stand out: the lack of a Miocene cooling event and the top-to- \sim E normal-sense
244 exhumation. We attribute the $\sim 45\text{--}30$ Ma rapid cooling as due to exhumation from $\sim 55\text{--}$

245 km-depth in a subduction-early collision setting at the leading edge of Greater India, as
246 observed in other THS rocks. The top-to-~E exhumation kinematics may indicate that the
247 Katha rocks were positioned at the easternmost end of the Himalaya.

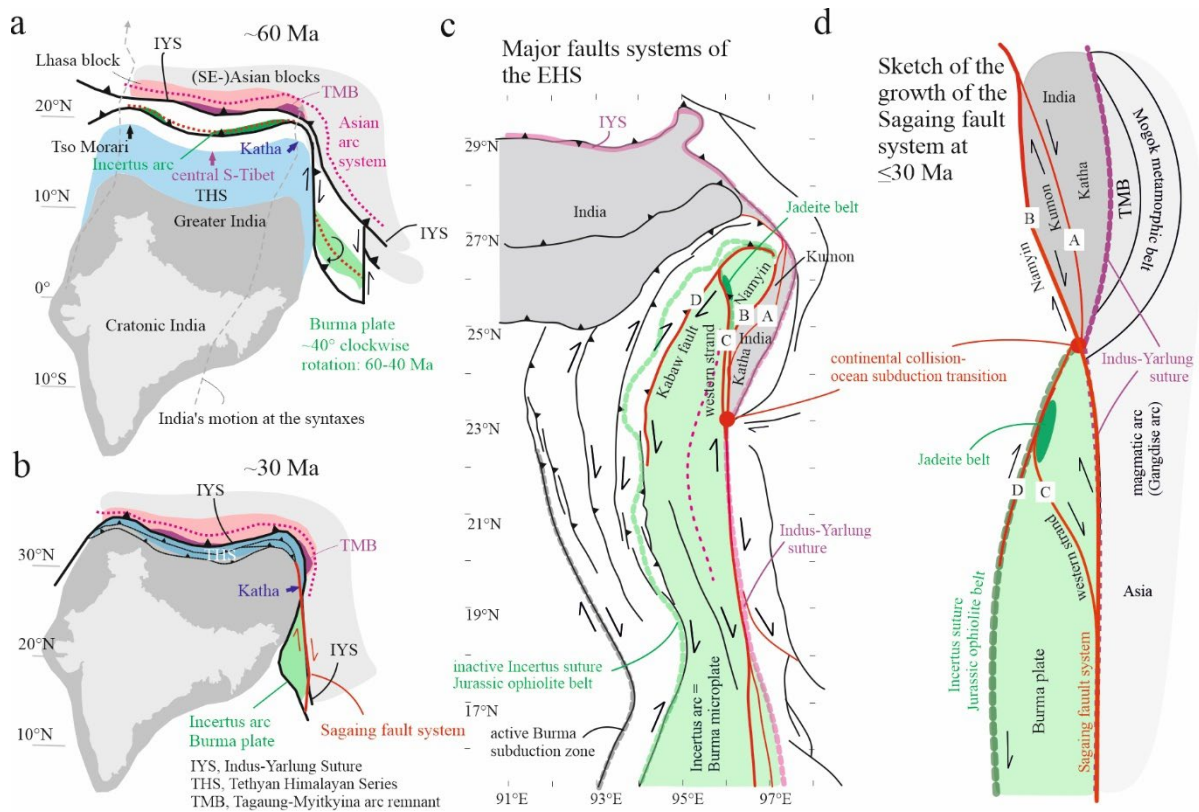
248

249 The initiation of the SF system has been bracketed to middle Miocene-early Pliocene,
250 based on the onset of seafloor spreading in the Andaman rift (e.g., [Bertrand & Rangin,](#)
251 [2003](#)). [Morley & Arboit \(2019\)](#) proposed a 28–27 Ma onset, based on the age of the basal
252 strata in a releasing-bend basin (Minwun basin, [Figure 1b](#)) along a SF strand in northern
253 Myanmar. The change from ~25 to ~4°C/Myr cooling of the Katha rocks at ~30 Ma may
254 signify their involvement into the SF system, when it started to interact with the THS
255 thrust-fold belt that acquired a ~N-strike during the northward propagation of India's
256 eastern tip. The movement around the EHS also allowed the Katha rocks to escape the
257 intense shortening at the collision front, thus a Miocene overprint.

258

259 [Figure 4](#) summarizes our proposed evolution of the EHS and the SF system: At ~60 Ma
260 ([Figure 4a](#)), the Incertus-arc system—which the Burma microplate was part of—
261 terminated ([Westerweel et al., 2019](#)). The highly-oblique plate boundary along Greater
262 India's eastern margin offset the Burma microplate (at ~5°N) from the leading Greater
263 India subduction in the north; collision with the Indian margin rotated it ~40° clockwise
264 (~60–40 Ma; [Li et al., 2020](#)). Continental subduction may have started at ≥47 Ma at both
265 syntaxes, as indicated in the western Himalaya (Tso Morari; [Donaldson et al., 2013](#)) and
266 the Katha range. The IYS at the eastern edge of the Burma microplate was reactivated as
267 the SF system ([Figure 4b](#)); its ~30 Ma initiation terminated the Katha-rock exhumation in
268 the subduction-collision setting and the transition to strike-slip motion with little
269 exhumation. The SF system connected with the THS thrust-fold belt at the EHS, where the

270 THS were later subducted together with the GHS (Haproff et al., 2020). Figures 4c and 4d
 271 show the evolution of the SF system: the eastern Namyin strand allows restoration of the
 272 Jadeite belt to the south, at least to the southern tip of the Indian rocks—south of the Katha
 273 Range; a western strand and the Kabaw fault allows restoration of the Jurassic ophiolite
 274 belt, connecting it to the south of the Jadeite belt. The entire area south of the EHS—
 275 including the SF system—experienced clockwise rotation and ~E-W shortening during
 276 the evolution of the Burma subduction system and the collision of the northward-moving
 277 Burma microplate with the Shillong plateau.



278
 279
 280 **Figure 4.** The Katha Range in the evolution of the Eastern Himalayan Syntaxis (EHS) and the Sagaing fault
 281 system (SF). a) Incipient Himalaya formation following Incertus-arc subduction with the Burma microplate
 282 at the arc's eastern end. b) Development of the SF system along the Indus-Yarlung suture (IYS) and its
 283 connection with the Tethyan-Himalaya fold-thrust belt. c) Major fault systems of the EHS. d) Restoration of
 284 the imbrication of the Incertus-arc subduction system at the western margin of the Burma microplate.

285 Growth of the SF system isolated the Jadeite belts and imbricated the Indian rocks of the Katha and Kumon
286 Ranges.

287

288 **Acknowledgments**

289 Funded by DFG RA 442/28.

290

291 **Conflict of Interest**

292 The authors declare no conflicts of interest relevant to this study.

293

294 **Open Research**

295 The petrologic and geo-thermochronologic data are available as Supporting Information
296 in the online version of this article and (CC-BY 4.0 license) on the OpARA server of TU
297 Bergakademie Freiberg and TU Dresden at <http://dx.doi.org/10.25532/OPARA-xxx> (will
298 be open when excepted).

299

300 **References**

301 Aikman, A.B., Harrison, T.M., & Ding, L. (2008). Evidence for early (>44 Ma) crustal

302 thickening, Tethyan Himalaya, southeastern Tibet. *Earth and Planetary Science*

303 *Letters*, 274, 14–23.

304 Aikman, A.B., Harrison, T.M., & Hermann, J. (2012). Age and thermal history of Eo- and

305 Neohimalayan granitoids, eastern Himalaya. *Journal of Asian Earth Sciences*, 51, 85–

306 97.

307 Baxter, A.T., Aitchison, J.C., Zybrev, S.V., & Ali, J.R. (2011). Upper Jurassic radiolarites

308 from the Naga ophiolite, Nagaland, northeast India. *Gondwana Research*, 20, 638–

309 644.

310 Bertrand, G., & Rangin, C. (2003). Tectonics of the western margin of the Shan Plateau
311 (central Myanmar): Implication for the India-Indochina oblique convergence since
312 the Oligocene. *Journal of Asian Earth Sciences*, 21, 1139–1157.

313 Blanckenburg, v. F., Villa, I.M., Baur, H., Morteani, G., & Steiger, R.H. (1989). Time
314 calibration of a PT-path from the Western Tauern Window, Eastern Alps: the
315 problem of closure temperatures. *Contributions Mineralogy Petrology*, 101, 1-11.

316 Bohlen, S.R., & Liotta J.J. (1986). A barometer for garnet amphiboles and garnet granulites.
317 *Journal of Petrology*, 27, 1025–1034.

318 Brandon, M.T., Roden-Tice, M.K., & Garver, J. I. (1998). Late Cenozoic exhumation of the
319 Cascadia accretionary wedge in the Olympic Mountains, northwest Washington
320 State. *Geological Society of America Bulletin*, 110, 985–1009.

321 Daniel, C.G., Hollister, L.S., Parrish, R.R., & Grujic, D. (2003). Exhumation of the Main
322 Central Thrust from lower crustal depths, eastern Bhutan Himalaya. *Journal*
323 *metamorphic Geology*, 21, 317–334.

324 De Capitani, C. (1994). Gleichgewichts-Phasendiagramme: Theorie und Software. *European*
325 *Journal of Mineralogy*, Bh.1, 6, 48.

326 Ding, H., Zhang, Z., Hu, K., Dong, X., Xiang, H., & Mu, H. (2016a). P-T-t-D paths of the North
327 Himalayan metamorphic rocks: Implications for the Himalayan orogeny.
328 *Tectonophysics*, 683, 393–404.

329 Ding, H., Zhang, Z., Dong, X., Tan, Z., Xiang, H., Mu, H., Gou, Z., Shui, X., Li, W., & Mao, L.
330 (2016b). Early Eocene (c. 50Ma) collision of the Indian and Asian continents:
331 Constraints from the North Himalayan metamorphic rocks, southeastern Tibet.
332 *Earth and Planetary Science Letters*, 435, 64–73.

333 Donaldson, D.G., Webb, A.A.G., Menold, C.A., Kylander-Clark, A.R.C., & Hacker, B.R.,
334 (2013). Petrochronology of Himalayan ultrahigh-pressure eclogite. *Geology*, *41*,
335 835–838.

336 Dunkl, I., Antolín, B., Wemmer, K., Rantitsch, G., Kienast, M., Montomoli, C., Din, L., Carosi,
337 R., Appel, E., El Bay, R., Xu, Q., & von Eynatten, H. (2011). Metamorphic evolution of
338 the Tethyan Himalayan flysch in SE Tibet. *Geological Society, Special Publications*,
339 *353*, 45–69.

340 Ewing, T.A., Rubatto, D., Beltrando, M., & Hermann, J. (2015). Constraints on the thermal
341 evolution of the Adriatic margin during Jurassic continental break-up: U–Pb dating
342 of rutile from the Ivrea–Verbano Zone, Italy. *Contribution Mineralogy Petrology*,
343 *169*, doi.org/10.1007/s00410-015-1135-6, 2015

344 Fang, D-R., Zhang, J., Hisada, K-I., Wang, G-H., & Li D. (2020). Geological anatomy of the
345 Upper Triassic sequence in southeastern Tibet: Implications for tectonic evolution
346 of the eastern Himalayan orogen. *Geological Journal*, *55*, 6607–6624.

347 Farley, K. A., Wolf, R. A., & Silver, L. T. (1996). The effects of long alpha-stopping distances on
348 (U-Th)/He dates. *Geochimica et Cosmochimica Acta*, *60*, 4223–4230.

349 Frei, D., & Gerdes A. (2009). Precise and accurate in situ U-Pb dating of zircon with high
350 sample throughput by automated LA-SF-ICP-MS. *Chemical Geology*, *261*, 261–270.

351 Gehrels, G., Kapp, P., DeCelles, P., Pullen, A., Blakey, R., Weislogel, A., Ding, L., Guynn, J.,
352 Martin, A., McQuarrie, N., & Yin, A. (2011). Detrital zircon geochronology of pre-
353 Tertiary strata in the Tibetan-Himalayan orogen. *Tectonics*, *30*,
354 <https://doi.org/10.1029/2011TC002868>

355 Ghent, E.D., Stout, M.Z., Black, P.M., & Brothers, R.N. (1987). Chloritoid bearing rocks with
356 blueschists and eclogites, northern New Caledonia. *Journal Metamorphic Geology*, *5*,
357 239–254.

358 Geological Map of Myanmar (2014). 1:2,250,000, Myanmar Geosciences Society.

359 Haproff, P.J., Zuza, A.V., & Yin, A. (2018). West-directed thrusting south of the eastern
360 Himalayan syntaxis indicates clockwise crustal flow at the indenter corner during
361 the India-Asia collision. *Tectonophysics*, 722, 277–285.

362 Haproff, P.J., Zuza, A.V., Yin, A., Harrison, T.M., Manning, C M., Ding, L., et al. (2019).
363 Geologic framework of the northern Indo-Burma Ranges: Lateral correlation of
364 Himalayan-Tibetan lithologic units across the eastern Himalayan syntaxis.
365 *Geosphere*, 15, 856–881.

366 Haproff, P.J., Odlum, M.L., Zuza, A.V., Yin, A., & Stockli, D.F. (2020). Structural and
367 thermochronologic constraints on the Cenozoic tectonic development of the
368 northern Indo-Burma Ranges. *Tectonics*, 39, e2020TC006231.
369 <https://doi.org/10.1029/2020TC006231>

370 Harrison, T.M., Célérier, J., Aikman, A.B., Hermann, J., & Heizler, M.T. (2009). Diffusion of
371 ⁴⁰Ar in muscovite. *Geochimica et Cosmochimica Acta*, 73, 1039–1051.

372 Hawthorne, F.C., Oberti, R., Harlow, G., Maresch, W.V., Martin, R.F., Schumacher, J.C., &
373 Welch, M.D. (2012). Nomenclature of the amphibole supergroup. IMA Report.
374 *American Mineralogist*, 97, 2031–2048.

375 Holdaway, M.J. (2000). Application of new experimental and garnet Margules data to the
376 garnet-biotite geothermometer. *American Mineralogist*, 85, 881–892.

377 Hu, X., Garzanti, E., Wang, J., Huang, W., & Webb, A.A.G. (2016). The timing of India–Asia
378 collision onset – facts, theories, controversies. *Earth-Science Reviews*, 160, 264–299.

379 Hynes, A., & Forest, R.C. (1988). Empirical garnet-muscovite geothermometry in low-grade
380 metapelites, Selwyn Range (Canadian Rockies). *Journal Metamorphic Geology*, 6, 297–
381 309.

382 Jarosewich, E., Nelen, J.A., & Norberg, J.A. (1980). Reference samples for electron
383 microprobe analysis. *Geostandard Newsletter*, 4, 43–47.

384 Käßner, A., Ratschbacher, L., Jonckheere, R., Enkelmann, E., Khan, J., Sonntag, B.-L.,
385 Gloaguen, R., Gadoev, M., & Oimahmadov, I. (2016). Cenozoic intracontinental
386 deformation and exhumation at the northwestern tip of the India-Asia
387 collision-southwestern Tian Shan, Tajikistan, and Kyrgyzstan. *Tectonics*, 35, 2171–2194.

388 Kooijman, E., Mezger, K., and Berndt, J. (2010). Constraints on the U–Pb systematics of
389 metamorphic rutile from in situ LA ICP-MS analysis. *Earth Planetary Science Letters*,
390 293, 321–330.

391 Kornfeld, D., Eckert, S., Appel, E., Ratschbacher, L., Sonntag, B.L., Pfänder, J.A., Ding, L., &
392 Liu, D. (2014). Cenozoic clockwise rotation of the Tengchong block, southeastern
393 Tibetan Plateau: a paleomagnetic and geochronologic study. *Tectonophysics*, 628,
394 105–122.

395 Kretz, R. (1983). Symbols for rock-forming minerals. *American Mineralogist*, 68, 277–279.

396 Kylander-Clark, A.R.C., Hacker, B.R., & Cottle, J.M. (2013). Laser-ablation split-stream ICP
397 petrochronology. *Chemical Geology*, 345, 99–112.

398 Laskowski, A.K., Kapp, P., Vervoort, J.D., & Ding, L. (2016). High-pressure Tethyan
399 Himalaya rocks along the India-Asia suture zone in southern Tibet. *Lithosphere*, 8,
400 574–582.

401 Laskowski, A.K., Kapp, P., Ding, L., Campbell, C., & Liu, X.H. (2017). Tectonic evolution of
402 the Yarlung suture zone, Lopu Range region, southern Tibet. *Tectonics*, 36, 108–
403 136.

404 Li, S., van Hinsbergen, D.J.J., Deng, C., Advokaat, E.L., & Zhu, R. (2018). Paleomagnetic
405 constraints from the Baoshan area on the deformation of the Qiangtang-Sibumasu

406 terrane around the eastern Himalayan syntaxis. *Journal of Geophysical Research,*
407 *Solid Earth, 123, 977–997.*

408 Li, Z., Ding, L., Zaw, T., Wang, H., Cai, F., Yao, W., Xiong, Z., Sein, K., & Yue, Y. (2020).
409 Kinematic evolution of the West Burma block during and after India-Asia collision
410 revealed by paleomagnetism. *Journal of Geodynamics, 134, 101690.*
411 <https://doi.org/10.1016/j.jog.2019.101690>

412 Linnemann, U., Ouzegane, K., Drareni, A., Hofmann, M., Becker, S., Gärtner, A., & Sagawe A.
413 (2011). Sands of west Gondwana: An archive of secular magmatism and plate
414 interactions—A case study from the Cambro-Ordovician section of the Tassili Ouan
415 Ahaggar (Algerian Sahara) using U-Pb-LA-ICP-MS detrital zircon ages. *Lithos, 123, 188–*
416 *203.*

417 Liu, C-Z., Chung, S-L., Wu, F-Y., Zhang C., Xu, Y., Wang, J-G., Chen, Y., & Gua, S. (2016).
418 Tethyan suturing in Southeast Asia: Zircon U-Pb and Hf-O isotopic constraints from
419 Myanmar ophiolites. *Geology, 44, 311–314.*

420 Ludwig, K.R. (2000). SQUID 1.00, A User's Manual. *Berkeley Geochronology Center Special*
421 *Publication, 2.*

422 Ludwig, K. (2008). User's Manual for Isoplot4.5. *Berkeley Geochronology Center Special*
423 *Publication, 4, 1-75.*

424 Maurin, T., Masson, F., Rangin, C., Min, U.T., & Collard, P. (2010). First global positioning
425 system results in northern Myanmar: constant and localized slip rate along the
426 Sagaing fault. *Geology, 38, 591–594.*

427 Mitchell, A. (2018). *Geological Belts, Plate Boundaries, and Mineral Deposits in Myanmar.*
428 Amsterdam, Netherlands, Elsevier, 524 p.

429 Morley, C.K., & Arboit, F. (2019). Dating the onset of motion on the Sagaing fault:
430 Evidence from detrital zircon and titanite U-Pb geochronology from the North
431 Minwun Basin, Myanmar. *Geology*, *47*, 581–585.

432 Paton, C., Hellstrom, J.C., Paul, B., Woodhead, J.D., & Hergt, J.M. (2011). Lolite: Freeware for
433 the visualisation and processing of mass spectrometer data. *Journal of Analytical*
434 *Atomic Spectrometry*, *26*, 2508–2518.

435 Pfänder, J. A., Sperner, B., Ratschbacher, L. Fischer, A., Meyer, M., & Leistner, M. (2014).
436 High-resolution $^{40}\text{Ar}/^{39}\text{Ar}$ dating using a mechanical sample transfer system combined
437 with a high-temperature cell for step heating experiments and a multi-collector ARGUS
438 noble gas mass spectrometer. *Geochemistry, Geophysics, Geosystems*, *15*, 2713–2726.

439 Pownceby, M.-I., Wall, V.-J., & O’Neill, H.S.C. (1987). Fe-Mn partitioning between garnet and
440 ilmenite; experimental calibration and applications. *Contributions to Mineralogy and*
441 *Petrology*, *97*, 116–126.

442 Qiu, Z., Wu, F.-Y., Yang, S.-F., Zhu, M., Sun, J.-F., & Yang, P. (2009). Age and genesis of the
443 Myanmar jadeite: constraints from U-Pb ages and Hf isotopes of zircon inclusions.
444 *Chinese Science Bulletin*, *54*, 658–668.

445 Ratschbacher, L., Frisch, W., Liu, G., & Chen, C.C. (1994). Distributed deformation in
446 southern and western Tibet during and after the India–Asia collision. *Journal*
447 *Geophysical Research*, *99*, 19,917–19,945.

448 Robinson, R.A.J., Brezina, C.A., Parrish, R.R., Horstwood, M.S.A., Nay Win Oo, Bird, M.I.,
449 Myint Thein, Walters, A.S., Oliver, G.J.H., & Khin Zaw (2014). Large rivers and
450 orogens: The evolution of the Yarlung Tsangpo–Irrawaddy system and the eastern
451 Himalayan syntaxis. *Gondwana Research*, *26*, 112–121.

452 Rutte, D., Pfänder, J.A., Kolečka, M., Jonckheere, R., & Unterricker, S. (2015). Radial fast-
453 neutron fluence gradients during rotating $^{40}\text{Ar}/^{39}\text{Ar}$ sample irradiation recorded with

454 metallic fluence monitors and geological age standards. *Geochemistry, Geophysics,*
455 *Geosystems, 16*, 336–345.

456 Rutte, D., Ratschbacher, L., Khan, J., Stübner, K., Hacker, B.R., Stearns, M.A., Enkelmann, E.,
457 Jonckheere, R., Pfänder, J.A., Sperner, B., & Tichomirowa, M. (2017) Building the Pamir-
458 Tibet Plateau—Crustal stacking, extensional collapse, and lateral extrusion in the
459 Central Pamir: 2. Timing and rates. *Tectonics, 36*, 385–419.

460 Salvi, D., Mathew, G., Kohn, B., Pande, K., & Borgohain, B. (2019). Thermochronological
461 insights into the morphotectonic evolution of Mishmi hills across the Dibang Valley,
462 NE Himalayan Syntaxis. *Journal of Asian Earth Sciences, 190*, 104158.
463 <https://doi.org/10.1016/j.jseaes.2019.104158>

464 Shi, G., Cui, W., Cao, S., Jian, N., Jian, P., Liu, D., Miao, L., & Chu, B. (2008). Ion microprobe
465 zircon U-Pb age and geochemistry of the Myanmar jadeitite. *Journal Geological*
466 *Society of London, 165*, 221–234.

467 Spear, F.S. (1993). *Metamorphic Phase Equilibria and Pressure-temperature-time Paths*.
468 Mineralogical Society of America Monographs, 799 pp.

469 Stübner, K., Ratschbacher, L., Weise, C., Chow, J., Hofmann, J., Khan, J., Rutte, D., Sperner, B.,
470 Pfänder, J.A., Hacker, B.R., Dunkl, I., Tichomirowa, M., & Stearns, M.A. (2013). The giant
471 Shakh dara migmatitic gneiss dome, Pamir, India-Asia collision zone: 2. Timing of dome
472 formation. *Tectonics, 32*, 1404–1431,

473 Thomas, J. B., Watson, E. B., Spear, F. S., Shemella, P. T., Nayak, S. K., & Lanzirrotti, A. (2010).
474 Titanite under pressure: The effect of pressure and temperature on the solubility of Ti
475 in quartz. *Contributions to Mineralogy and Petrology, 160*, 743–759.

476 Van Hinsbergen, D.J.J., Lippert, P.C., Dupont-Nivet, G., McQuarrie, N., Doubrovine, P.V.,
477 Spakman, W., & Torsvik, T.H. (2012). Greater India basin hypothesis and a two-

478 stage Cenozoic collision between India and Asia. *Proceedings of the National*
479 *Academy of Science, 109*, 7659–7664.

480 Wauschkuhn, B., Jonckheere, R., & Ratschbacher, L. (2015). The KTB apatite fission-track
481 profiles: Building on a firm foundation? *Geochimica et Cosmochimica Acta, 167*, 27–62.

482 Westerweel, J., Roperch, P., Licht, A., Dupont-Nivet, G., Win, Z., Poblete, F., Ruffet, G., Swe,
483 H.H., Thi, M.K., & Aung, D.W. (2019). Burma terrane part of the Trans-Tethyan arc
484 during collision with India according to paleomagnetic data. *Nature Geoscience, 12*,
485 863–868.

486 Wang, E., & Burchfiel, B.C. (1997). Interpretation of Cenozoic tectonics in the right-
487 lateral accommodation zone between the Aialo Shan shear zone and the Eastern
488 Himalayan Syntaxis. *International Geological Review, 39*, 191–219.

489 Warren, C.J., Hanke, F., & Kelley, S.P. (2012). When can muscovite $^{40}\text{Ar}/^{39}\text{Ar}$ dating
490 constrain the timing of metamorphic exhumation? *Chemical Geology, 291*, 79–86.

491 Wiedenbeck, M., Alle, P., Corfu, F., Griffin, W.L., Meier, M., Oberli, F., Von Quadt, A.,
492 Roddick, J.C., & Spiegel, W. (1995). Three natural zircon standards for U-Th-Pb, Lu-Hf,
493 trace element and REE analyses. *Geostandards Newsletter, 19*, 1-23.

494 Williams, I.S. (1998). U-Th-Pb geochronology by ion microprobe. *Reviews in Economic*
495 *Geology, 7*, 1-35.

496 Yang, J.S., Xu, Z.Q., Duan, X.D., Xiong, F.H., Liu, Z., Cai, Z.H., & Li, H.Q. (2012). Discovery of a
497 Jurassic SSZ ophiolite in the Myitkyina region of Myanmar. *Acta Petrologica Sinica,*
498 *28*, 1710–1730.

499 Zhang, P.Z., Shen, Z., Wang, M., Gan, W., Bürgmann, R., Molnar, P., Wang, Q., Niu, Z., Sun, J.,
500 Wu, J., & Hanrong, S. (2004). Continuous deformation of the Tibetan Plateau from
501 global positioning system data. *Geology, 32*, 809–812.

502 Zhang, J., Xiao, W., Windley, B.F., Wakabayashi, J., Cai, F., Seing, K., Wu, H., & Naing, S.
503 (2018). Multiple alternating forearc- and backarc-ward migration of magmatism in
504 the Indo-Myanmar Orogenic Belt since the Jurassic: Documentation of the orogenic
505 architecture of eastern Neotethys in SE Asia. *Earth-Science Reviews*, 185, 704–731.

506 Zubovich, A.V., Wang, X Q., Scherba, Y.G., Schelochkov, G.G., Reilinger, R., Reigber, C., et al.
507 (2010). GPS velocity field of the Tien Shan and surrounding regions. *Tectonics*, 29,
508 TC6014. <https://doi.org/10.1029/2010TC002772>